ELSEVIER

International Journal of Solids and Structures 41 (2004) 1645–1675

INTERNATIONAL JOURNAL OF SOLIDS and STRUCTURES

www.elsevier.com/locate/ijsolstr

Aluminum foam-filled extrusions subjected to oblique loading: experimental and numerical study

A. Reyes *, O.S. Hopperstad, M. Langseth

Structural Impact Laboratory (SIMLab), Department of Structural Engineering, Norwegian University of Science and Technology, Rich. Birkelands vei 1A, N-7491 Trondheim, Norway

Received 7 January 2003; received in revised form 12 September 2003

Abstract

The behavior of empty and foam-filled square thin-walled aluminum columns in alloy AA6060 subjected to quasi-static oblique loading was examined. Previous studies have shown that by introducing a load angle, the energy absorption decreases drastically compared to axial loading. One of the main objectives of the present investigation was to study the effect of introducing aluminum foam filler on the energy absorption. The square columns were clamped at one end and oblique load conditions were realized at the other end by applying a force with different angles to the centerline of the column. An experimental program was carried out where the main parameters were load angle, foam density and heat treatment of the extrusion material. Additionally, numerical analyses of the experiments were performed, mainly to verify a numerical model of the obliquely loaded foam-filled columns. The foam was modeled with the foam model of Deshpande and Fleck, together with a simple fracture criterion, which previously has been implemented as a user subroutine in LS-DYNA. The study shows that high-density aluminum foam filler increases the energy absorption considerably, but the specific energy absorption is lowered compared to the empty cross sections. Furthermore, the numerical analyses were able to predict the experimental results with reasonable accuracy.

Keywords: Combined loading; Thin-walled foam-filled column; Aluminum extrusions; Aluminum foam

1. Introduction

Structural collapse of thin-walled members in axial folding has been the subject of both academic and industrial research over the last decades. Energy-absorbing systems consisting of different tubular parts, often including crash boxes, are frequently used in vehicles to protect passengers and the car's structure during impact. The crash boxes are designed to control the initial kinetic energy of the car during impact, and at the same time avoid permanent deformations in the rest of the car body by keeping the force

* Corresponding author. Tel.: +47-73-59-45-24; fax: +47-73-59-47-01.
E-mail address: aase.reyes@bygg.ntnu.no (A. Reyes).

0020-7683/$ - see front matter © 2003 Elsevier Ltd. All rights reserved.
doi:10.1016/j.ijsolstr.2003.09.053

Nomenclature

θ	load angle
$\Delta\theta$	additional rotation from initial position
F_{max}	peak force
F_{mean}	mean crush load
d	displacement in direction of the force
A_E	crush force efficiency
T_E	total efficiency
d_{max}	displacement at maximum value of T_E
S_E	stroke efficiency
ρ_f, ρ_{f0}	foam density and foam base material density
ρ_{al}	density of aluminum
$\bar{\sigma}$	average stress
σ_p	plateau stress
C_{pow}	power-law coefficient
n	material constant
l	component length
b	outer cross section width of extrusion
b_i	inner cross section width of extrusion $= b - 2h$
b_m	mean cross section width of extrusion $= b - h$
h	component wall thickness
Tx	temper x. Heat treatment of extrusion
F	crush force in direction of the load
E	absorbed energy, Young's modulus
σ	true stress
$\sigma_{0.2}$	stress at 0.2% plastic strain
σ_u	ultimate stress
σ_0	characterstic stress
ε	true strain
σ_{eng}	engineering stress
ε_{eng}	engineering strain
$\bar{\varepsilon}$	engineering strain corresponding to maximum total efficiency
ε_0	engineering strain at maximum engineering stress level
C_{avg}, C_{max}	interaction constants of average and peak force for axial crushing
m	mass
SEA	specific energy absorption
N	axial force
M	moment
σ_0, c_i, q_i	material parameters for extrusion material
Φ	yield function
$\hat{\sigma}$	equivalent stress
Y	yield stress
α	shape factor in material model for foam
α_2, γ, β	material parameters for foam
ε_D	compaction strain

v^p	plastic coefficient of contraction
C_0, C_1, n	material constants for foam
w_0	amplitude of initial imperfection
$v(t)$	velocity field
t	time
T	total duration of loading

levels sufficiently low. A high-speed crash may activate a larger part of the structure in order to absorb all of the energy. The crash boxes deform, and consequently deformations and forces are transferred to the rest of the structure, which may lead to both bending and axial loading of other structural parts. Pure bending and axial crushing of square columns have been subject to extensive studies, resulting in expressions for mean forces and bending moments (Kecman, 1983; Jones, 1989; Wierzbicki et al., 1994).

Steel has been the traditional material in the automotive industry, but the weight of aluminum makes it attractive because of the advantages a lighter vehicle gives. Weight savings of 25% can be achieved when using aluminum instead of conventional steel structures, which will reduce fuel consumption and lower emission of carbon dioxide. Tubes made from aluminum extrusions show good energy-absorbing capability when exposed to axial crushing: energy is absorbed through extensive folding of the sidewalls of the crash boxes. Nevertheless, the energy absorber will seldom be subjected to either pure axial or bending collapse during a crash event, but rather a combination of the two modes. Requirements in the automotive industry demand that the bumper system should endure a load applied in a 30° load angle to the longitudinal axis. In an oblique crash, the crash boxes will be subjected to both axial forces and moments. Previous studies (Reyes et al., 2002, 2003) show that the columns may experience global bending collapse instead of progressive buckling, and, consequently, the energy absorption will be significantly lowered, while both moments and axial forces will be transferred to the rest of the vehicle's structure.

Some investigations regarding oblique loading of tubular members have been carried out even if studies in this area are limited. Han and Park (1999) investigated numerically columns of mild steel impacted at a declined rigid wall with no friction. Different angles were tested, and the response was divided into axial collapse, bending collapse and a transition zone. An empirical expression for the critical angle was found. Kim and Wierzbicki (2001) explored numerically the crush behavior of columns subjected to combined bending and compression, by prescribing both displacements and rotations at the upper end of a cantilever column. They found that the failure loci shrink for increasing deformation, and that an analytical model was able to predict the numerical results. Previous studies by Reyes et al. (2002, 2003) of thin-walled aluminum extrusions subjected to oblique loading showed that the energy absorption drops drastically by introducing a load angle of 5° compared to the axial crushing. This is due to the different collapse modes, as the progressive buckling of axial crushing is a much more energy-absorbing process than bending. The studies also showed that the energy absorption increased by increasing the wall thickness, and this changed the characteristics of the force–displacement curves. A different approach to increase the energy absorption could be to fill the hollow columns with aluminum foam.

Aluminum foam can be suitable as a filler material for extrusions, and can increase the energy-absorbing capability of a crash box, without adding too much mass. Extensive studies have been carried out on the crushing behavior of foam-filled columns with various cross sections subjected to axial loading (Reid et al., 1986; Abramowicz and Wierzbicki, 1988; Santosa, 1997; Seitzberger et al., 1997; Santosa and Wierzbicki, 1998; Hanssen et al., 1999, 2000b), both numerically and experimentally. The energy absorption was

certainly increased by adding foam filler, but so was the mass. The performance of foam-filled compared to empty columns varied in the different studies, due to different measures of performance (Hanssen et al., 2001), various foam qualities, geometry and so on.

The effect of foam in beams subjected to bending has also been subject to both experimental and numerical studies. An experimental study by Hanssen et al. (2000a) showed that the presence of foam filler increased the energy absorption compared to empty beams drastically. Santosa and Wierzbicki (1999) studied the effect of aluminum foam on bending collapse of thin-walled aluminum extrusions and found that the specific energy absorption was significantly higher for foam-filled sections than for empty columns. Santosa et al. (2000, 2001) looked at fully and partially foam-filled steel beams and found that the energy absorption of foam-filled beams was considerably greater than the energy absorption of the empty beams. Chen (2001) investigated deep bending collapse of thin-walled empty and foam-filled hat profiles, and found that the specific energy absorption of partially filled columns was increased by 30–40% compared to non-filled members. The study of Chen et al. (2002) showed that the foam-filled columns subjected to bending and bending/compression performed much better than empty columns.

Numerical simulations using a finite element program such as LS-DYNA (Hallquist, 1998) are required in vehicle design, and a suitable material model for the aluminum foam is therefore important. In the aforementioned numerical studies of foam-filled tubes (Santosa, 1997; Santosa and Wierzbicki, 1999; Santosa et al., 2000, 2001; Chen, 2001), a one-dimensional plasticity model in PAM-CRASH was used to model the foam, while the foam plasticity model in ABAQUS was used by Seitzberger et al. (1997). Hanssen et al. (2002) carried out a validation study where different available foam models in LS-DYNA were tested. One of the conclusions was that the existing models were unable to represent all load configurations because of lack of a suitable fracture criterion.

As foam filler seems to increase the energy absorption in both axial compression and bending, the behavior of square thin-walled aluminum columns filled with aluminum foam subjected to oblique loading is here investigated experimentally. Extrusions with a slightly thinner wall thickness than in previous studies (Reyes et al., 2002, 2003) were chosen. Two different foam densities were examined, and empty columns with the same wall thickness were tested for reference. Load angle and heat treatment of the alloy (temper) were also varied. The main objectives of the present study on obliquely loaded foam-filled tubes were to examine the effects of aluminum foam filler on the energy-absorbing capability, and to increase the experimental database for obliquely loaded cantilever columns. The experiments also served as basis for validation of a numerical model of foam-filled columns subjected to oblique loading, and numerical analyses of the experiments were carried out. The foam was in the present study modeled with the foam model of Deshpande and Fleck (2000), which has earlier been implemented as a user subroutine in LS-DYNA (Reyes, 2003; Reyes et al., 2003).

2. Terminology

Fig. 1 shows how oblique loading was realized in the present study. The test specimen was clamped at the lower end, and the quasi-static force was applied through a rigid body at the upper end of the specimen. Due to the test set-up, some variation of the applied load angle, θ, was observed during testing. The variation in load angle was less than 2°, and can be considered negligible.

Force–displacement curves from an axially crushed tube and an obliquely loaded tube that experiences global bending is shown in Fig. 2. The global bending mode was observed for all experiments in the present project, but measures introduced for axial crushing are applied for the evaluation of the results, and the terminology from Hanssen et al. (2000b) is applied in the present study. Some useful parameters are therefore defined in the following. Integration of the force vs. deformation curve gives the energy

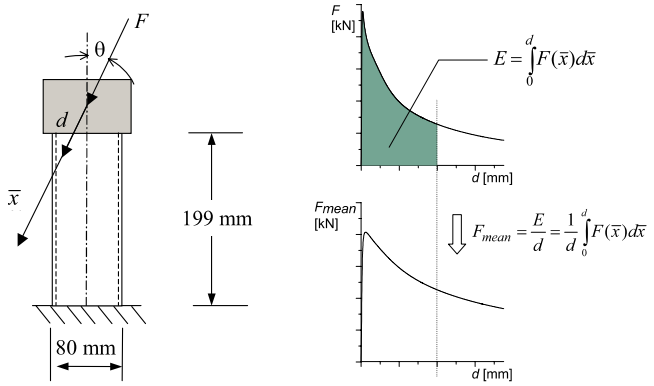

Fig. 1. Oblique loading of column.

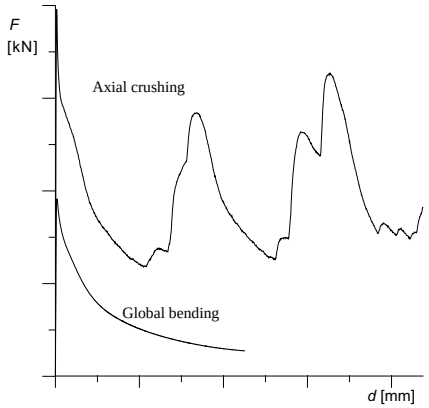

Fig. 2. Typical force–displacement curves for axial crushing and global bending of empty thin-walled columns.

absorption for the corresponding deformation. The mean crush load, $F_{\text{mean}}(d)$, is defined as the absorbed energy divided by the current deformation (see Fig. 1), while the maximum force in the domain $[0, d]$ is here called $F_{\max}$. The ratio of $F_{\text{mean}}(d)$ to $F_{\max}$ is defined as the crush force efficiency, $A_{\text{E}}(d)$, and the total efficiency is defined as

$$T_{\text{E}}(d) = \frac{F_{\text{mean}}(d)}{F_{\max}} \frac{d}{l} = A_{\text{E}}(d) \frac{d}{l} \tag{1}$$

where l is the initial length of the specimen. The maximum deformation $d_{\max}$ is defined as the displacement that corresponds to the maximum value of the total efficiency, while the maximum deformation divided by the length is referred to as the stroke efficiency, S_{E}:

$$S_{\text{E}} = \frac{d_{\max}}{l} \tag{2}$$

3. Material properties

3.1. Extrusion material

The square columns were made of aluminum alloy AA6060, tempers T4 and T6. Although the columns fail by local buckling in the compression flange, standard tensile tests were used to establish the stress–strain curves. This was guided by tests performed by Opheim (1996) who found no significant difference in the behavior in tension and compression of the present material. The test specimens were taken out parallel to the extrusion direction, and the material tests of T4 were performed within the same weeks as the component tests to avoid any effect of age hardening. Fig. 3 shows typical engineering stress–strain curves for the alloy used, while Table 1 summarizes the average values of mechanical properties obtained in the material tests. There was not much discrepancy in the results from the tensile tests, the stress levels varied within 5%. Note that the values of Young's modulus, E, in Table 1, are smaller than the nominal value of 70,000 MPa for aluminum, and this is probably caused by imperfections in geometry and alignment of the test specimens.

3.2. Foam

The aluminum foam used in the tests was manufactured by Hydro Aluminium AS with the melt gas injection method (Ashby et al., 2000). This method results in foams with relative densities between 0.03 and 0.1. Two densities of the aluminum foam were applied in the experiments, with nominal values $\rho_{f1} = 0.1$ g/cm^3 and $\rho_{f2} = 0.3$ g/cm^3. Uniaxial compression tests of square cubes of foam were performed to determine the power-law relationship (Gibson and Ashby, 1997)

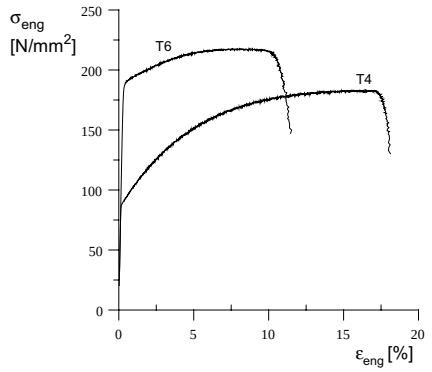

Fig. 3. Typical engineering stress–strain curves of extrusion material, tempers T4 and T6.

Table 1
Mechanical properties of extrusion material (based on the engineering stress–strain curves)

Temper	h [mm]	$\sigma_{0.2}$ [N/mm^2]	σ_u [N/mm^2]	E [N/mm^2]
T4	1.74	91	185	64,750
T6	1.76	189	217	66,502

$$\sigma_{\mathrm{p}} = C_{\mathrm{pow}} \left(\frac{\rho_{\mathrm{f}}}{\rho_{\mathrm{f0}}} \right)^{m} \tag{3}$$

between foam density, ρ_{f} and foam plateau stress, σ_{p} (see Fig. 4). C_{pow} and m are material constants dependent upon foam type, while ρ_{f0} is the density of the foam base material, which is 2.7 g/cm^3 for aluminum. The dimensions of the cubes were $70\times70\times70$ mm^3, and five parallel tests were performed in three directions. The directions are defined as: x:casting direction, y: transverse directions and z: the thickness direction. In order to establish the density of the foam, the test specimens were measured and weighed prior to testing.

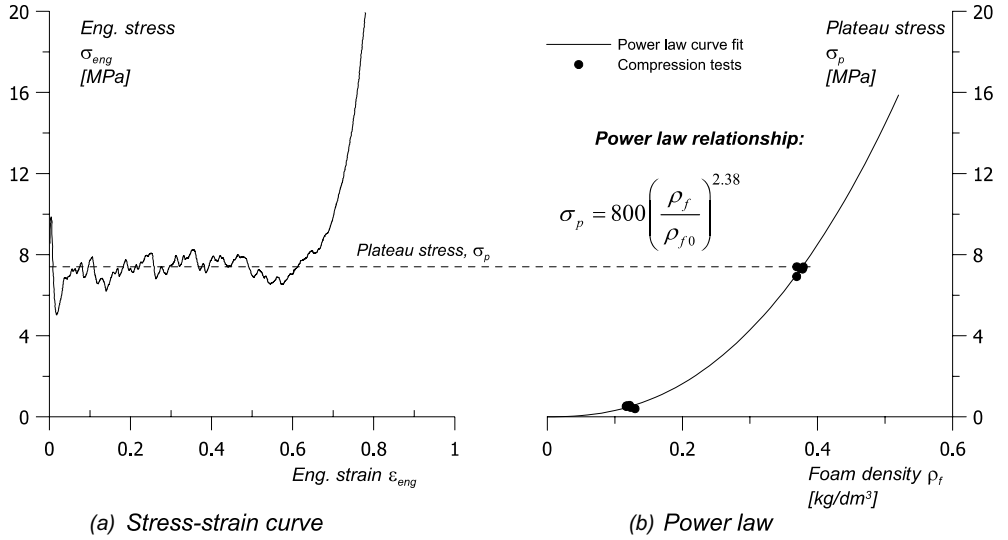

Fig. 4. Mechanical behavior of aluminum foam in uniaxial compression. (a) Stress–strain curve, (b) power law.

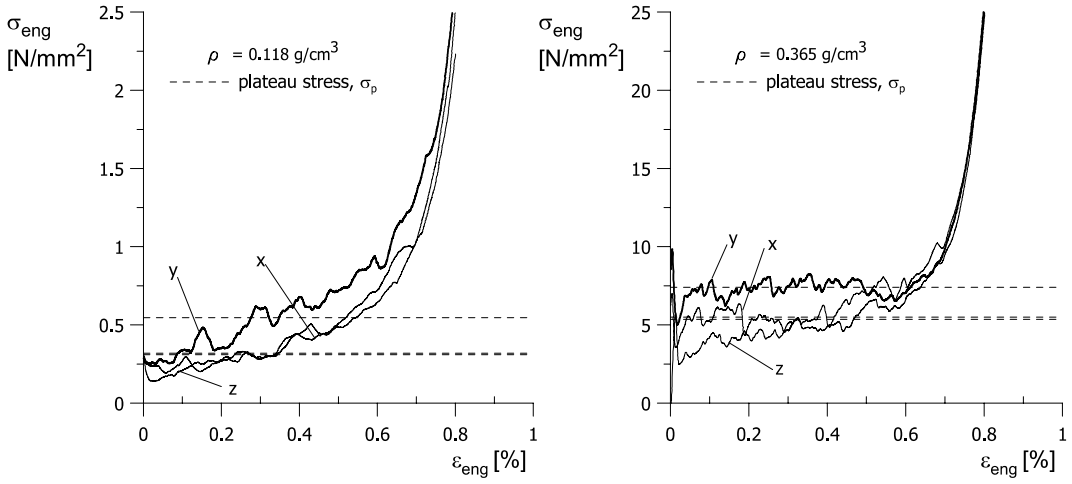

Fig. 5. Stress–strain curves of aluminum foam.

The plateau stress, σ_p was determined for each compression test as $\sigma_p = \frac{1}{\bar{\varepsilon}_{eng}} \int_0^{\bar{\varepsilon}_{eng}} \sigma_{eng} d\varepsilon_{eng}$. σ_{eng} and ε_{eng} are the engineering stress and strain, respectively, and $\bar{\varepsilon}_{eng}$ is the engineering strain corresponding to maximum total efficiency, $T_{E,max}$. The results from the uniaxial compression tests were fitted to Eq. (3), and the constants were found to be $C_{pow} = 800$ MPa and $m = 2.38$. The power law is shown in Fig. 4b together with the experimental results, which show some scatter. Because of this scatter, the power-law relationship was important to determine the actual plateau stress of the foam used in the extrusions.

Fig. 5 depicts typical stress–strain curves from quasi-static uniaxial compression tests on aluminum foam cubes in three different directions. As one can see, the aluminum foam in the present study clearly shows anisotropic behavior, which is mainly caused by the manufacturing procedure, as the foam is produced as a sheet material during a continuous casting process, and gravity and other parameters influence solidification of the cell structure (Hanssen et al., 2000b). One can see that the material has higher strength in the y-direction than in the other two directions. This was also observed by Hanssen et al. (2002), who explained this by the fact that the cells have the major extension along the y-axis. In the present study the foam's y-direction was aligned in the longitudinal direction of the tube as in previous studies on axially loaded foam-filled tubes (Hanssen et al., 2000b,c). It was therefore decided to use the foam properties in the same direction. To avoid unnecessary scatter in the test results due to the anisotropic behavior, all the data points in Fig. 4 refer to the properties in the y-direction, and the power law was fitted to these data.

4. Experimental program and test set-up

Table 2 shows the test program together with the test specimen's geometry and support conditions. Tests of axially loaded ($\theta = 0°$) square foam-filled tubes which collapsed progressively have previously been performed by Hanssen et al. (2000b). Due to the test set-up in the present study, however, the tubes could go into bending failure even when loaded axially. It was therefore decided only to apply the load with an angle to the longitudinal axis.

The free length, width and wall thickness of the test specimens were constant. In order to ensure clamping at the lower end and a uniform loading at the upper end, the length of the extrusions was longer than the free length, and the lower and upper part was internally filled with a steel and wood block, respectively (see Fig. 6). The foam was machined and inserted into the empty columns with its y-direction aligned with the longitudinal direction of the column. Two values of the foam density were used, and empty

Table 2
Test program

Alloy	Temper	Wall thickness, h [mm]	Angle, θ [°]	Foam density, ρ_f [g/cm^3]
AA6060	T4		5	0
	T6	1.7	15	0.1
			30	0.3

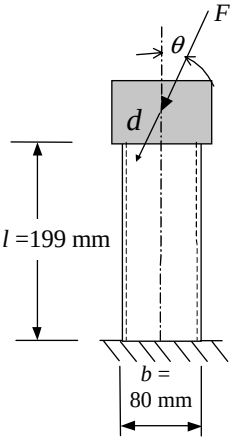

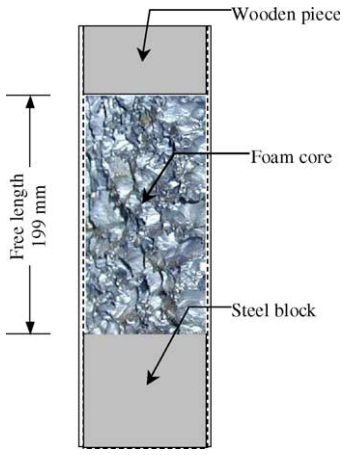

Fig. 6. Placement of foam core in extrusion.

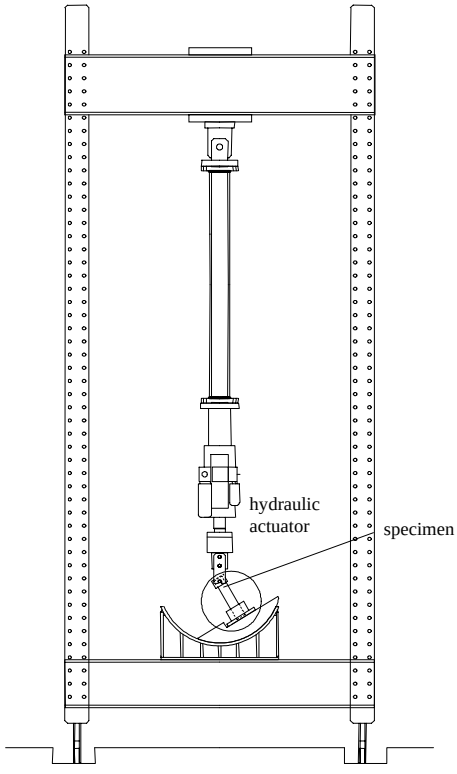

Fig. 7. Test rig.

columns were also tested. With three parallel tests for each combination of foam density, temper (heat treatment of alloy), and load angle, a total of 54 tests were performed. Peak force and mean crush load were the response parameters.

As the material tests of the foam showed considerable scatter, all the columns were weighed and measured before and after the foam was inserted. Thus, the foam density for every column was calculated, and the plateau stress could be calculated from the power law (Eq. (3)). The wall thickness of the specimens was measured prior to testing, and the variation in thickness relative to the average value was less than 5%. The following identification system was adopted: S–T–θ–h–x–n, where S stands for static test, T is the temper, θ is the load angle, h is the thickness, x stands for foam density no. x, and n is repetition no. n. Here, foam density no. 0 means an empty column, while foam density nos. 1 and 2 correspond to $\rho_{f1} = 0.114$ g/cm^3 and $\rho_{f2} = 0.301$ g/cm^3, respectively.

The test specimens were clamped at the lower end and free at the top before applying the load. The tests were performed in the same test rig (see Fig. 7) that has been applied in earlier studies (Reyes et al., 2002, 2003). The rig was purpose-built for testing columns subjected to oblique, quasi-static loading. It consists of a "cradle", a hydraulic actuator and a supporting frame. A moving part in the cradle can be fixed at the desired angle to a stationary part. In order to obtain an almost conservative load situation, the loading device (actuator and column) was made as long as possible. Due to height limitations in the laboratory, the length of the loading device was about 3650 mm giving some variation (less than 2°) of the applied load angle, θ.

During testing, the applied load was measured using a load cell, while the displacement was measured by a video extensometer, which recorded the coordinates of different points that were all in the same plane. The coordinates of the point at which the load was applied gave at all times the displacement in x- and y-direction. From the test set-up, it was possible to calculate the displacement in the direction of the force. All tests were quasi-static and the displacement was applied at a constant speed of 500 mm/h.

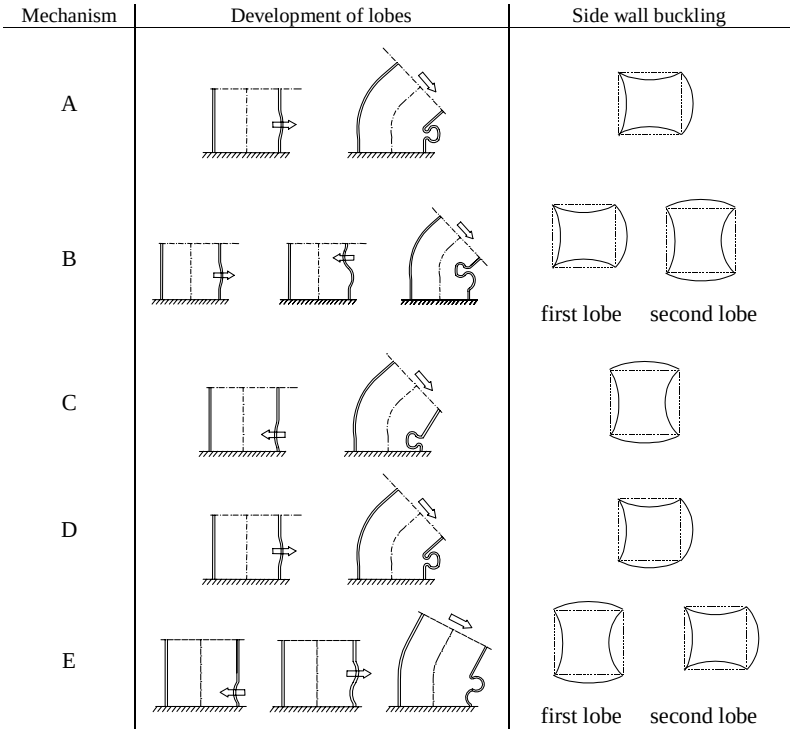

Fig. 8. Deformation modes.

Table 3
Summary of experiments, T4

Test no.	Load angle θ [°]	Extrusion material					Foam		Response parameters		Deformation mode
		Width b [mm]	Thickness h [mm]	Yield stress $\sigma_{0.2}$ [N/mm^2]	Ultimate stress σ_u [N/mm^2]	Characterstic stress σ_0 [N/mm^2]	Density ρ [g/cm^3]	Plateau stress σ_p [N/mm^2]	Peak force F_{max} [kN]	Mean force[a] F_{mean} [kN]	
S-T4-5-1.7-0-1	5	80	1.73	91	183	158	0	0	31.12	9.07	A
S-T4-5-1.7-0-2	5	80	1.74	91	183	158	0	0	31.23	9.46	C
S-T4-5-1.7-0-3	5	80	1.73	91	183	158	0	0	29.40	8.28	C
S-T4-15-1.7-0-1	15	80	1.74	91	183	158	0	0	17.34	7.20	E
S-T4-15-1.7-0-2	15	80	1.74	91	183	158	0	0	17.45	7.26	E
S-T4-15-1.7-0-3	15	80	1.73	91	183	158	0	0	17.78	7.38	C
S-T4-30-1.7-0-1	30	80	1.74	91	189	159	0	0	11.04	6.63	E
S-T4-30-1.7-0-2	30	80	1.73	91	189	159	0	0	11.21	6.40	E
S-T4-30-1.7-0-3	30	80	1.74	91	189	159	0	0	11.46	6.81	E
S-T4-5-1.7-1-1	5	80	1.75	91	189	159	0.105	0.35	29.94	10.52	C
S-T4-5-1.7-1-2	5	80	1.75	91	189	159	0.104	0.34	32.97	10.86	A
S-T4-5-1.7-1-3	5	80	1.74	91	189	159	0.123	0.52	32.32	9.37	C
S-T4-15-1.7-1-1	15	80	1.74	92	189	162	0.100	0.31	18.44	8.69	A
S-T4-15-1.7-1-2	15	80	1.74	92	189	162	0.118	0.46	18.50	8.30	A
S-T4-15-1.7-1-3	15	80	1.74	92	189	162	0.110	0.39	18.75	8.19	B
S-T4-30-1.7-1-1	30	80	1.74	92	189	162	0.096	0.28	11.40	6.75	A
S-T4-30-1.7-1-2	30	80	1.74	92	189	162	0.112	0.41	11.19	7.16	E
S-T4-30-1.7-1-3	30	80	1.74	92	189	162	0.121	0.49	11.67	7.31	A
S-T4-5-1.7-2-1	5	80	1.76	89	180	155	0.302	4.35	38.39	22.14	A*
S-T4-5-1.7-2-2	5	80	1.75	89	180	155	0.277	3.56	37.07	19.54	E
S-T4-5-1.7-2-3	5	80	1.75	89	180	155	0.344	5.92	43.07	27.16	A*
S-T4-15-1.7-2-1	15	80	1.76	89	180	155	0.331	5.43	20.17	15.33	A*
S-T4-15-1.7-2-2	15	80	1.76	89	180	155	0.285	3.80	20.15	15.71	A*
S-T4-15-1.7-2-3	15	80	1.75	89	180	155	0.305	4.45	20.56	15.67	A*
S-T4-30-1.7-2-1	30	80	1.74	91	183	158	0.281	3.68	12.76	11.10	E*
S-T4-30-1.7-2-2	30	80	1.74	91	183	158	0.336	5.60	13.53	12.25	A*
S-T4-30-1.7-2-3	30	80	1.72	91	183	158	0.295	4.13	12.68	11.46	E*

[a] The mean force is calculated for a displacement of 50 mm.

5. Experimental results

5.1. Visual observations

For all the specimens, the compression flange buckled, and the peak load was then reached followed by a global bending mode giving a plastic hinge close to the clamped support. After the hinge was developed, the column rotated around the hinge as a rigid body. The development of the first lobe varied somewhat in the experiments: the compression flange would buckle either inward or outward. Five typical deformation modes were observed, which are here called mechanism A, B, C, D, and E. The deformation modes of the foam-filled columns were similar to the modes in previous studies of oblique loading. Fig. 8 shows the different deformation modes schematically. Although the plastic hinge always was developed at the lower end of the column, there was some variation in the distance from the bottom of the column to the first lobe. The deformation mode for each test is given in Tables 3 and 4. Mechanism B was only seen once, while mechanism D, an asymmetric mode, was observed only three times. Deformation modes A, E and C were

Table 4
Summary of experiments, T6

Test no.	Load angle θ [°]	Extrusion material					Foam		Response parameters		Deformation mode
		Width b [mm]	Thickness h [mm]	Yield stress $\sigma_{0.2}$ [N/mm^2]	Ultimate stress σ_u [N/mm^2]	Characterstic stress σ_0 [N/mm^2]	Density ρ [g/cm^3]	Plateau stress σ_p [N/mm^2]	Peak force F_{max} [kN]	Mean force[a] F_{mean} [kN]	
S-T6-5-1.7-0-1	5	80	1.76	187	215	201	0	0	57.93	13.02	C
S-T6-5-1.7-0-2	5	80	1.76	187	215	201	0	0	60.57	11.91	C
S-T6-5-1.7-0-3	5	80	1.76	187	215	201	0	0	58.46	12.37	C
S-T6-15-1.7-0-1	15	80	1.76	187	215	201	0	0	33.97	10.56	A
S-T6-15-1.7-0-2	15	80	1.77	187	215	201	0	0	32.85	10.20	C
S-T6-15-1.7-0-3	15	80	1.77	187	215	201	0	0	32.52	10.28	C
S-T6-30-1.7-0-1	30	80	1.76	193	219	205	0	0	20.59	9.19	C
S-T6-30-1.7-0-2	30	80	1.76	193	219	205	0	0	20.38	8.97	C
S-T6-30-1.7-0-3	30	80	1.76	193	219	205	0	0	20.19	9.23	C
S-T6-5-1.7-1-1	5	80	1.76	193	219	205	0.125	0.53	58.58	13.91	C
S-T6-5-1.7-1-2	5	80	1.76	193	219	205	0.111	0.41	55.21	14.42	C
S-T6-5-1.7-1-3	5	80	1.76	193	219	205	0.105	0.35	58.42	12.93	C
S-T6-15-1.7-1-1	15	80	1.76	188	218	204	0.131	0.59	32.57	11.03	C
S-T6-15-1.7-1-2	15	80	1.76	188	218	204	0.113	0.42	32.00	11.07	C
S-T6-15-1.7-1-3	15	80	1.76	188	218	204	0.129	0.58	33.33	11.87	C
S-T6-30-1.7-1-1	30	80	1.76	188	218	204	0.120	0.48	20.72	9.65	C
S-T6-30-1.7-1-2	30	80	1.76	188	218	204	0.125	0.54	21.31	10.68	E
S-T6-30-1.7-1-3	30	80	1.76	188	218	204	0.120	0.49	20.89	10.24	C
S-T6-5-1.7-2-1	5	80	1.77	187	216	202	0.283	3.73	68.20	28.20	A**
S-T6-5-1.7-2-2	5	80	1.77	187	216	202	0.301	4.30	66.98	25.03	D
S-T6-5-1.7-2-3	5	80	1.77	187	216	202	0.294	4.08	64.39	24.28	E
S-T6-15-1.7-2-1	15	80	1.77	187	216	202	0.299	4.26	36.59	20.31	D
S-T6-15-1.7-2-2	15	80	1.77	187	216	202	0.320	5.00	36.35	19.22	A
S-T6-15-1.7-2-3	15	80	1.77	187	216	202	0.311	4.67	36.55	19.98	D
S-T6-30-1.7-2-1	30	80	1.77	191	219	204	0.277	3.55	22.06	12.34	A
S-T6-30-1.7-2-2	30	80	1.76	191	219	204	0.332	5.47	22.27	15.34	E
S-T6-30-1.7-2-3	30	80	1.76	191	219	204	0.306	4.50	22.63	14.14	A

[a] The mean force is calculated for a displacement of 50 mm.

the most common mechanisms, and C occurred mostly for the empty columns in temper T6 and the columns with the lowest density foam in temper T6. For the other experiments, the deformation mode seemed to be random. Some pictures of the different deformation modes are given in Fig. 9. Some of the mechanisms appear similar, but the development of the lobes was somewhat different. Mechanism A**, which is depicted in Fig. 9, was a strange variation of mechanism A. The lobe buckled outward, and at the same time, there was created outward lobes in the webs just below the outward lobe in the flange.

The foam-filled and empty columns developed similar deformation modes. Fig. 10 shows three specimens with various foam filler in temper T4 with load angle 5°. Here, the compression flange buckled outward, while the two sidewalls buckled inward. Although the specimens in Fig. 10 have the same deformation mode in the sense that the compression wall buckled outward, one can see that there are some differences in the extent of the lobe, which can be considered as a plastic hinge. The lobes in the foam-filled columns are somewhat more localized than in the empty columns, in agreement with the findings of Hanssen et al. (2000b). The foam acts as an elastic–plastic foundation for the sidewalls and reduces their buckling length.

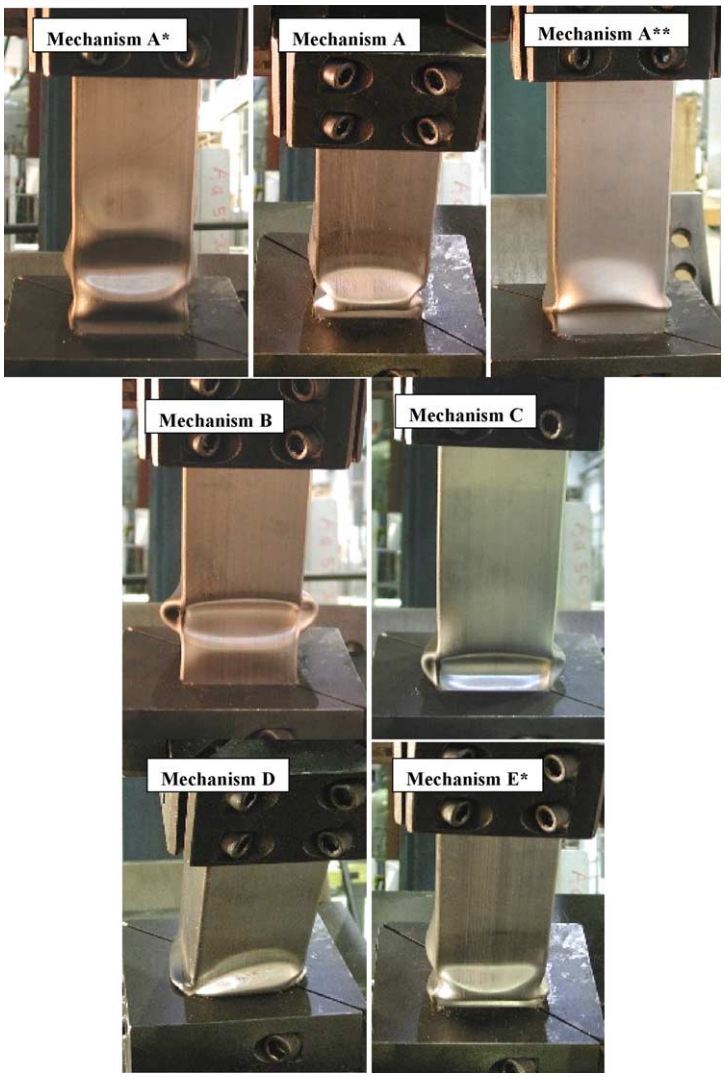

Fig. 9. Pictures from experiments: S-T4-15-1.7-2-3 (A*), S-T4-30-1.7-1-3 (A), S-T6-5-1.7-2-1 (A**), S-T4-15-1.7-1-3 (B), S-T4-15-1.7-0-3 (C), S-T6-15-1.7-2-1 (D), S-T4-30-1.7-2-3 (E*).

A detail of the tube with high-density (0.3 g/cm^3) foam is shown in Fig. 11. It is possible to see an indication of a second lobe above the initial lobe. This was also observed for some of the other tubes with high-density foam. The indication of a second lobe is denoted A* or E* in Tables 3 and 4.

5.2. General behavior

The measured peak and mean forces from the experiments are given in Tables 3 and 4, together with the specific material data for foam and extrusion for each specimen. The mean loads were calculated at a displacement of $d = 50$ mm $\approx 0.25 \cdot l$, and the plateau stresses were calculated from the power law, as

Fig. 10. Deformation modes for experiment $\theta = 5°$, temper T4, empty, and foam densities 0.1 and 0.3 g/cm^3.

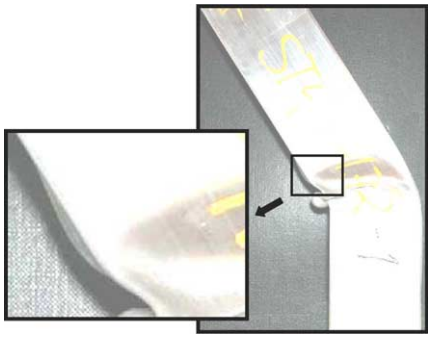

Fig. 11. Detail of S-T4-5-1.7-2-1.

mentioned earlier. The characteristic stress σ_0 for the extrusion material is here defined as (Abramowicz and Jones, 1986)

$$\sigma_0 = \left\{ \int_0^{\varepsilon_0} \sigma_{\text{eng}}(\varepsilon_{\text{eng}})\, \mathrm{d}\varepsilon_{\text{eng}} \right\} \Big/ \varepsilon_0 \tag{4}$$

where ε_0 is the engineering strain at maximum engineering stress.

Fig. 12 shows typical force vs. displacement curves from the experiments. Tests with the same temper and load angle are plotted in the same diagram. The behavior of the empty columns is as expected similar to previous tests; for a load angle of 5°, a drastic drop in force level follows the very high peak force corresponding to the buckling of the compression flange. The peak loads decrease for larger angles, but the force level does not fall as quickly as for 5°. The columns filled with no foam and low-density foam ($\rho_f \approx 0.1$ g/cm^3) have very similar behavior, i.e. the foam does not have much influence. However, the high-density foam has a large effect on the force–displacement curves. For $\theta = 30°$ and temper T4, for instance, the force maintains almost the same level for the whole displacement after reaching the maximum force. The mean load and the peak force vs. load angle are depicted in Fig. 13. As one can see, the low-density foam increases the mean load slightly (5–15%), while the high-density foam increases the mean load between 50% and 100%. The largest increase occurs for $\theta = 5°$. The mean loads also decrease for increasing load angles. The peak

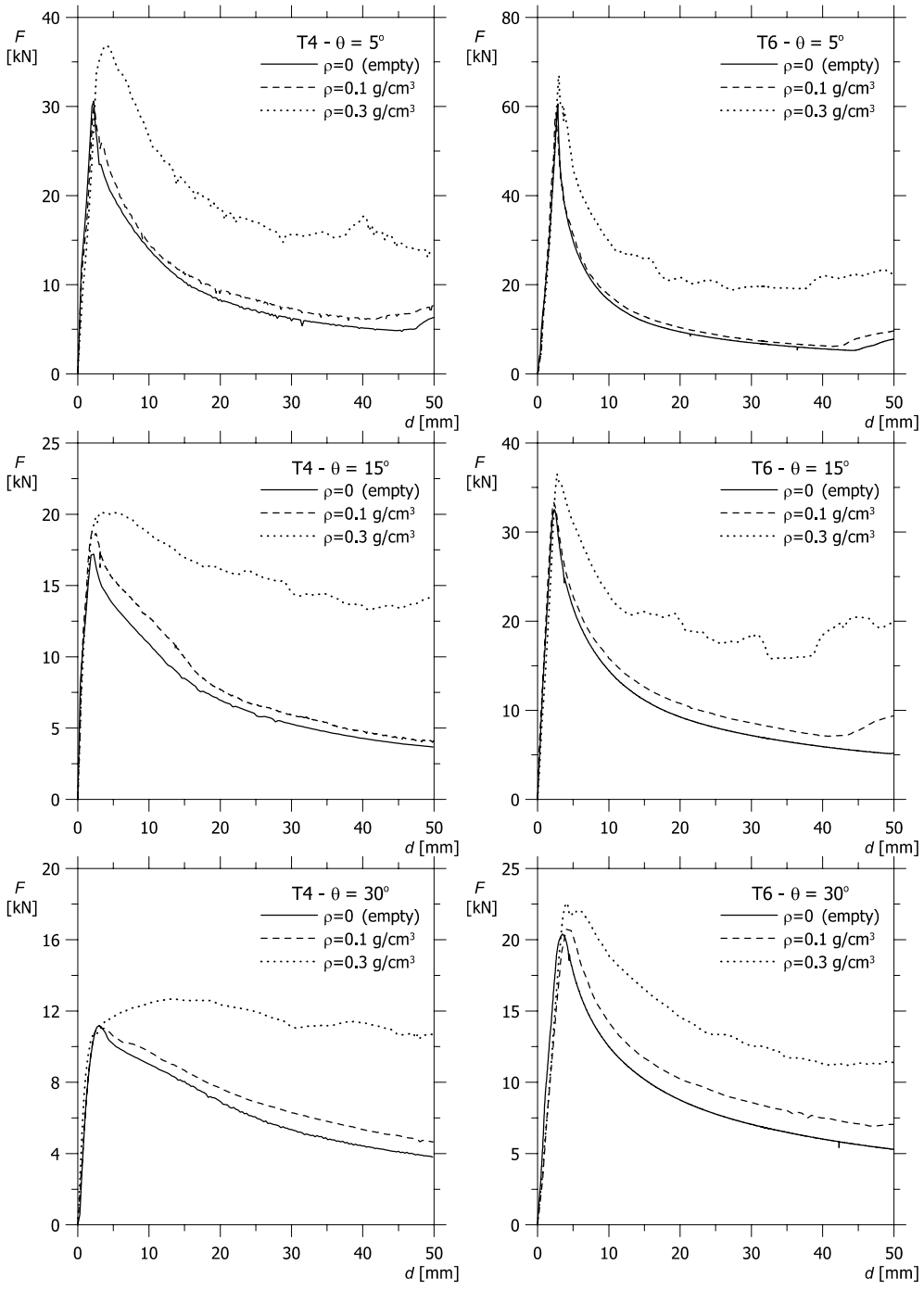

Fig. 12. Applied force vs. displacement of typical tests.

loads are not affected much by the low-density foam filler, but increases somewhat for the high-density foam. The peak loads decrease for increasing load angles.

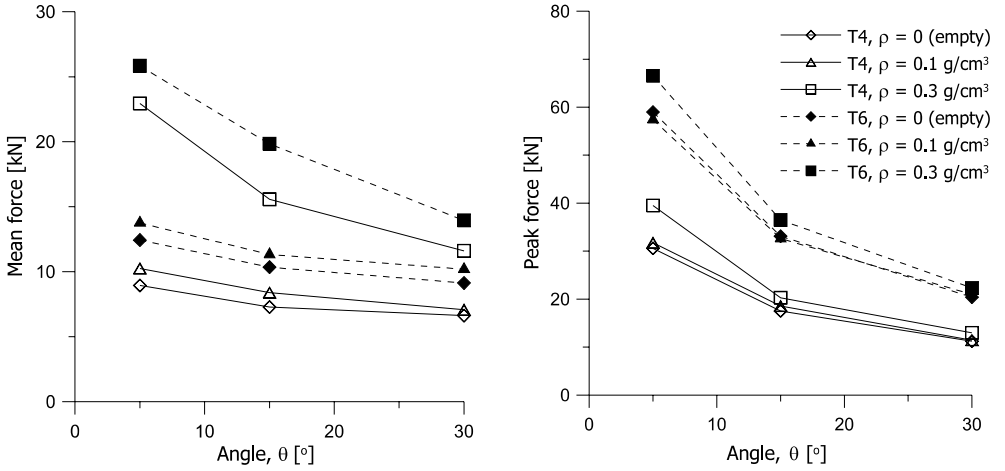

Fig. 13. Mean load at $d = 50$ mm and peak load vs. load angle.

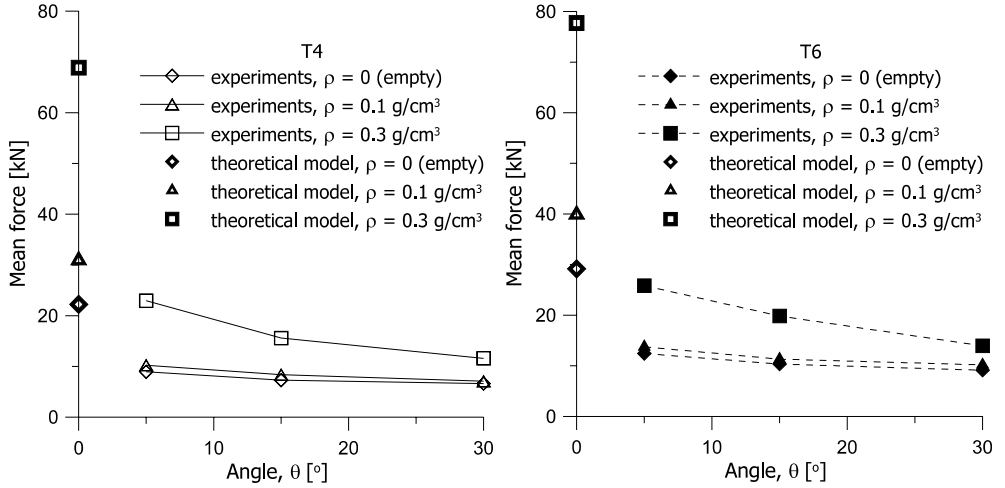

Fig. 14. Mean load at $d = 50$ mm vs. load angle. The calculated mean crushing force for an axially loaded column is also included.

The mean crushing force of empty, axially loaded columns, proposed by Abramowicz and Jones (1986) for a rigid plastic material, is defined as

$$F_{\text{mean}} = 13.06\sigma_0 \cdot h^2 \cdot \left(\frac{b_{\text{m}}}{h}\right)^{1/3} \tag{5}$$

σ_0 is here taken as the characteristic stress defined in Eq. (4) to account for the hardening in the material. Hanssen et al. (2000b) suggested an expression for the mean crushing force for an axially loaded foam-filled column as

$$F_{\text{mean}} = 13.06\sigma_0 \cdot h^2 \cdot \left(\frac{b_{\text{m}}}{h}\right)^{1/3} + \sigma_{\text{p}} b_{\text{i}}^2 + C_{\text{avg}}\sqrt{\sigma_{\text{p}}\sigma_0} b_{\text{m}} h \tag{6}$$

Here, σ_p is the plateau stress of the foam, b_i and b_m are the inner and mean width defined as $b_i = b - 2h$ and $b_m = b - h$, and C_{avg} is a constant. Similarly, an expression for the maximum force for a foam-filled column subjected to axial loading, was also proposed by Hanssen et al. (2000b):

$$F_{max} = \frac{1}{A_{E0}} 13.06\sigma_0 \cdot h^2 \cdot \left(\frac{b_m}{h}\right)^{1/3} + \frac{1}{A_{Ef}} \sigma_p b_i^2 + C_{max}\sqrt{\sigma_p \sigma_0} b_m h \tag{7}$$

where A_{E0} and A_{Ef} are the crush force efficiency for respectively the extrusion alone and the foam alone. The mean and peak loads for axially loaded columns were calculated from Eqs. (5)–(7) to find the corresponding values for progressive folding. Guided by Hanssen et al. (2000b), the constants were set to $C_{avg} = 5.5$, $C_{max} = 1.96$, $A_{E0} = 0.48$ and $A_{Ef} = 0.85$. The calculated mean crushing forces and peak loads for axially loaded columns, using Eqs. (5)–(7), together with the experimental results are shown in Figs. 14 and 15. As one can see, the mean loads drop drastically by introducing a load angle of just 5°, for both empty and foam-filled columns. One can also see how the peak loads drop when going from progressive buckling to global bending. However, the constants in Eq. (7) are dependent on triggers and initial imperfections, so these are mainly estimates to give an idea of the values for progressive buckling.

After the peak load was reached in the experiments, a hinge was formed in the column and the cross section was distorted compared to its original shape, and subsequently the rest of the column rotated as a rigid body. This additional rotation $\Delta\theta$ of the column from its initial position was calculated, together with the axial forces and moments at the bottom of the column. Fig. 16 shows interaction plots for each temper and foam density from all the experiments, for equal values of $\Delta\theta$. An interaction curve that represents one value of $\Delta\theta$ can be described as the failure locus for that deformation (Kim and Wierzbicki, 2001). The points corresponding to the maximum forces are also included in the figures for reference although these points do not represent the same additional rotation. The load paths of the experiments are plotted as well, and show the relationship between moments and axial forces at all times.

As one can see, the interaction curves of the empty columns and the specimens with the low-density foam are similar. The columns loaded with a 5° load angle have the highest axial forces and the moment is almost constant through the experiment for temper T4 for $\rho = 0$ and $\rho = 0.1$ g/cm^3. For temper T6 the moment decreases somewhat. For the two other load angles, 15° and 30°, the moment is much higher, both moments and axial forces decrease with increasing rotation, and the reduction in moment is quite large from the

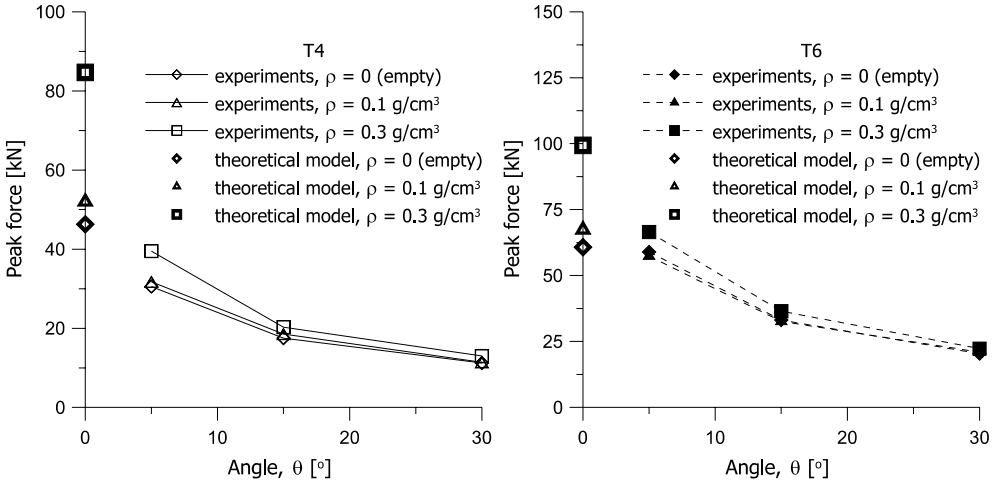

Fig. 15. Peak load vs. load angle. The calculated maximum crushing force for an axially loaded column is also included.

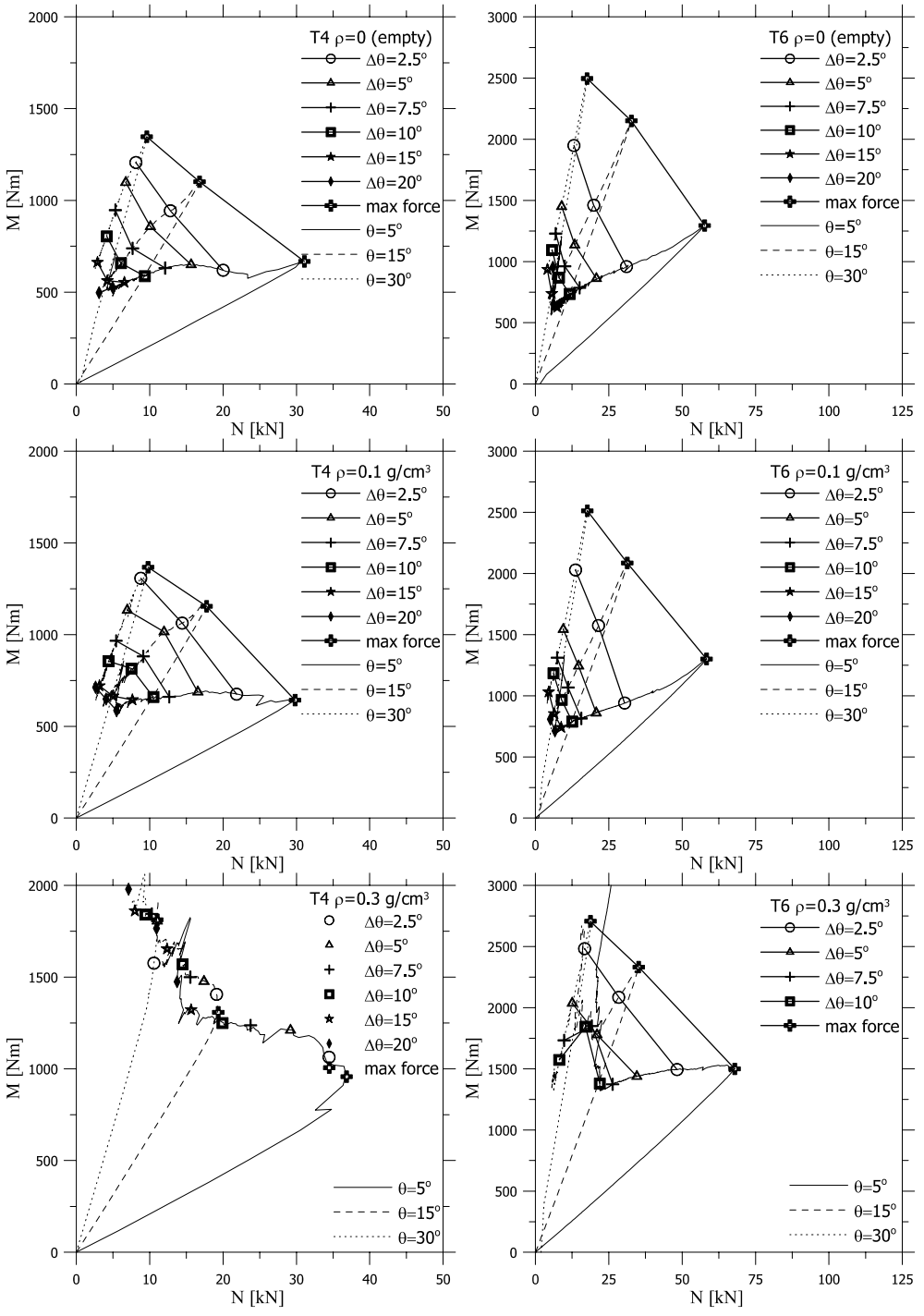

Fig. 16. Interaction plots for equal additional rotation $\Delta\theta$ from typical experimental results.

point corresponding to the maximum force until the end of the experiment. One can also see from the curves that as in previous studies (Reyes et al., 2003), the failure loci shrink as the rotation progresses.

The interaction curves for temper T6 with a foam density of 0.3 g/cm^3 have similar characteristics to the interaction curves for empty tubes and tubes filled with low-density foam. The axial force is highest for $\theta = 5°$, and for this load angle the moment is almost constant while the axial force decreases. However, when the additional rotation is equal to or larger than 10°, the moment increases while the axial force is almost constant. This is also the case for $\theta = 15°$.

The test specimens in temper T4 filled with foam with $\rho_f \approx 0.3$ g/cm^3 have very different interaction curves than the others. The axial force for $\theta = 5°$ is decreasing, but the moment is not constant for increasing rotation, but rather increasing. The result of this behavior is that the failure loci for increasing rotation do not shrink as for the other experiments, but stay at the same place. No explanation for this behavior has been found, and thus further investigations are needed.

5.3. Mass efficiency

As the experimental results show, the energy absorption and maximum loads increase when going from an empty cross section to a foam-filled one, and the gain is greatest for the energy absorption for specimens with the high-density foam ($\rho_f \approx 0.3$ g/cm^3). However, the foam filler contributes to the mass, and makes the test specimens with foam filler heavier than the empty ones. Previous studies on empty columns subjected to oblique loading by Reyes et al. (2003) showed that the energy absorption and peak loads increased for increasing wall thickness for all load angles. In that study, the wall thickness was varied from 1.9 to 4.5 mm, and the increase in wall thickness leads of course to a higher weight for the specimens.

One question that arises is whether the performance of obliquely loaded columns can be improved by adding foam filler compared to simply increasing the wall thickness of the cross section. The answer depends on how performance is measured. The energy absorption is of course important. However, the maximum force that will be transferred to the rest of the structure is also significant. The crush force efficiency evaluates the ratio of the maximum force to the mean load, while the specific energy absorption is defined as the energy absorption divided by the mass. In the following, these different measures are presented for the experiments. The mass is simply calculated as $m = 4b_m hl\rho_{al} + b_i^2 l\rho_f$. Since the length is the same for all the tests, the mass to length ratio is sometimes used. The mean loads are calculated at

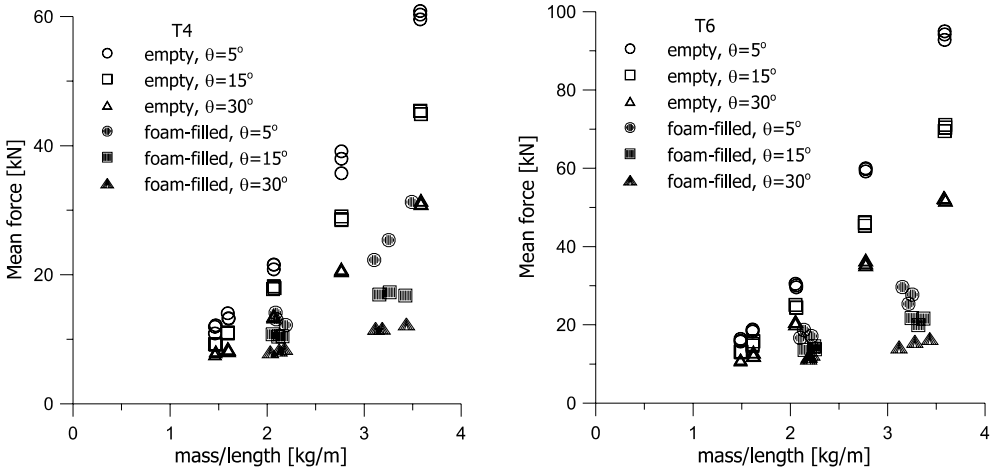

Fig. 17. Mean force at $d = 30$ mm vs. mass/length ratio, results for empty and foam-filled cross sections.

$d = 30$ mm to be able to compare with the results from the previous study (Reyes et al., 2003). All the figures include the experimental results from Reyes et al. (2003) for comparison.

The mean loads vs. the mass to length ratio are presented in Fig. 17. As one can see from the figure, the increase in mass for the empty columns gives a much higher mean force than the approximately same increase in mass for the foam-filled columns.

Fig. 18 depicts the peak loads vs. the mass to length ratio. The peak force increases a great deal for the empty columns with increasing wall thickness, while the maximum loads for a foam-filled cross section with the approximately same weight are much smaller.

The crush force efficiency, $A_E = F_{mean}/F_{max}$ is plotted versus the mass to length ratio in Fig. 19. The crush force efficiency is generally higher for the empty cross sections than for the foam-filled ones. However, for

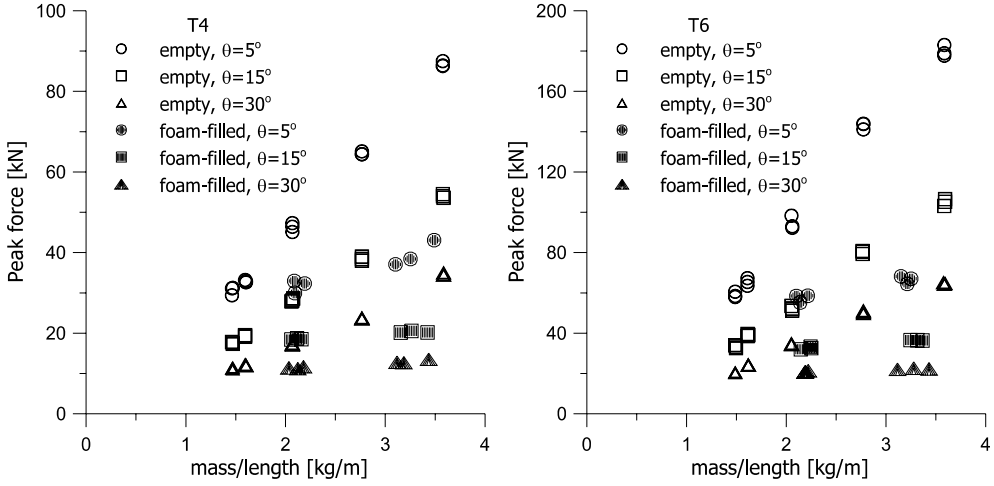

Fig. 18. Maximum force vs. mass/length ratio, results for empty and foam-filled cross sections.

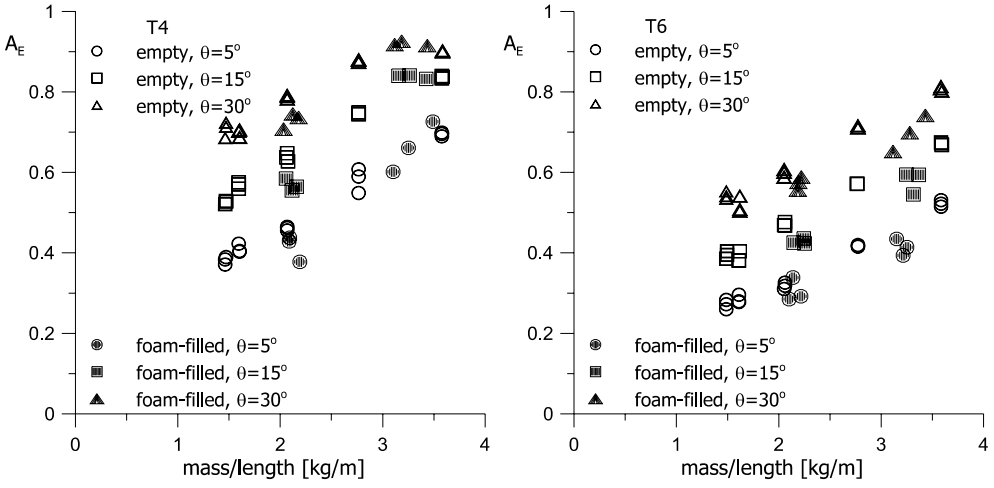

Fig. 19. Crush force efficiency at $d = 30$ mm vs. mass/length ratio, results for empty and foam-filled cross sections.

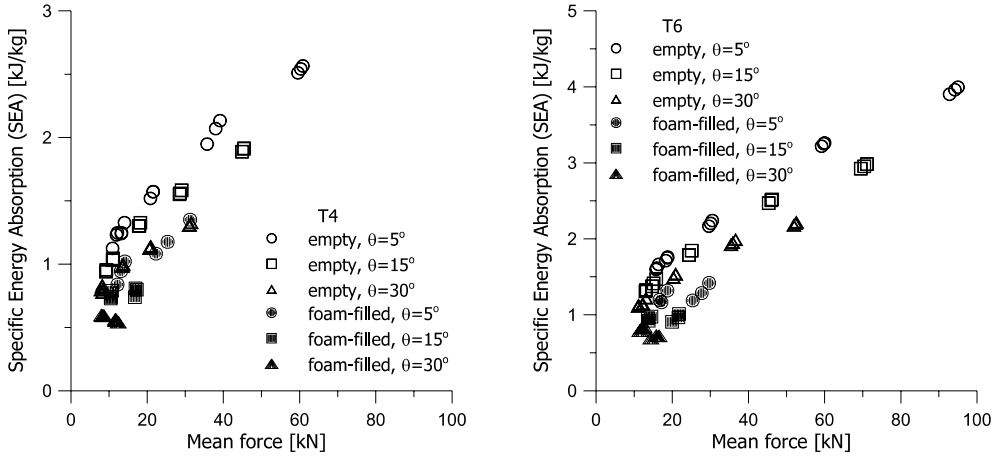

Fig. 20. Specific energy absorption vs. mean force, results for empty and foam-filled cross sections.

the columns in temper T4, it seems like the crush force efficiency for the empty and foam-filled columns approach each other for a mass to length ratio greater than 3.

The specific energy absorption (SEA) was calculated for a displacement of 30 mm, and is plotted vs. the mean force in Fig. 20. It is clear that for the same mean force, SEA is higher for the empty columns.

As previous studies have shown (Santosa et al., 2000, 2001; Chen, 2001), a higher mass efficiency can be obtained by partial foam filling at the locations where the plastic hinges can be expected. However, the basis for the present investigation was the crash box that can be subjected to oblique as well as pure axial loading. When loaded axially, the tube should be fully filled, and that is why partial foam filling was not investigated here.

6. Numerical analyses

All the experiments were analyzed with LS-DYNA (Hallquist, 1998), using the numerical model from previous studies (Reyes et al., 2002, 2003) as a basis for the simulations.

6.1. Material modeling

6.1.1. Extrusion material

The extrusion material was modeled with material model 103 in LS-DYNA (Berstad et al., 1994; Hopperstad and Remseth, 1995), where Hill's yield criterion, the associated flow rule, and combined nonlinear isotropic and kinematic hardening are adopted. In the present study, isotropy is assumed, which leads to the von Mises yield criterion, and further isotropic hardening is adopted. The constitutive relation is defined by

$$\sigma_e = \sigma_0 + q_1[1 - \exp(-c_1\varepsilon_e)] + q_2[1 - \exp(-c_2\varepsilon_e)] \tag{8}$$

where σ_e and ε_e is the von Mises effective stress and strain respectively; σ_0 is the proportionality limit, c_i govern the rate of change in the hardening variables and q_i represent their asymptotic values.

The uniaxial true stress–strain behavior of representative material tests was for each temper fitted to Eq. (8), and Table 5 contains the material constants σ_0, c_i and q_i ($i = 1, 2$).

Table 5
Material constants for extrusion material

Parameter	T4	T6
E [N/mm^2]	63,485	65,841
σ_0 [N/mm^2]	86.65	177.3
Q_1 [N/mm^2]	138.5	59.63
Q_2 [N/mm^2]	0.52	10.63
C_1	15.75	20.70
C_2	744.3	1684

6.1.2. Aluminum foam

The aluminum foam was modeled with the foam model of Deshpande and Fleck (2000), which has been implemented as a user subroutine in LS-DYNA (Reyes, 2003; Reyes et al., 2003). The implemented model includes a simple fracture criterion, and reasonable results were obtained when this model was used in verification tests on foam alone. The anisotropy of the foam is not taken into account in the foam model.

The yield criterion of the material model is given as

$$\Phi = \hat{\sigma} - Y \leqslant 0 \tag{9}$$

where

$$\hat{\sigma}^2 = \frac{1}{[1 + (\alpha/3)^2]}[\sigma_e^2 + \alpha^2 \sigma_m^2] \tag{10}$$

Here, σ_m is the mean stress and the parameter α defines the shape of the yield surface. α is a function of the plastic coefficient of contraction, v^p:

$$\alpha^2 = \frac{9}{2}\frac{(1 - 2v^p)}{(1 + v^p)} \tag{11}$$

Since v^p can be assumed to be zero for the aluminum foams considered in the current study (Reyes et al., 2003), α is equal to $\sqrt{9/2} \approx 2.12$.

The material model includes the following isotropic strain-hardening rule:

$$Y = \sigma_p + R(\hat{\varepsilon}) = \sigma_p + \gamma\frac{\hat{\varepsilon}}{\varepsilon_D} + \alpha_2 \ln\left(\frac{1}{1 - (\hat{\varepsilon}/\varepsilon_D)^\beta}\right) \tag{12}$$

Here, $\hat{\varepsilon}$ is the equivalent plastic strain, while σ_p, α_2, γ, ε_D, and β are material parameters. If the strain hardening rule is calibrated to a uniaxial compression test, the compaction strain, ε_D, can be expressed as (Reyes et al., 2003)

$$\varepsilon_D = -\frac{9 + \alpha^2}{3\alpha^2} \ln\left(\frac{\rho_f}{\rho_{f0}}\right) \tag{13}$$

where ρ_f is the foam density and ρ_{f0} is the density of the base material, which is 2.7 g/cm^3 for aluminum. The other material properties, σ_p, α_2, γ, and β, can also be expressed as a function of the foam density:

$$\left\{\sigma_p, \alpha_2, \gamma, \frac{1}{\beta}\right\} = C_0 + C_1\left(\frac{\rho_f}{\rho_{f0}}\right)^n \tag{14}$$

where C_0, C_1, and n are constants (Hanssen et al., 2002).

The material tests were used to determine the power-law relationship between foam density, ρ_f, and foam plateau stress, σ_p which is expressed in Eq. (14) with $C_0 = 0$. Furthermore, the values of C_0, C_1, and n

Table 6
Material constants for aluminum foam

Parameter	σ_p	γ	α	$1/\beta$	W
C_0 [N/mm^2]	0	0	0	0.22	0
C_1 [N/mm^2]	800	40	140	320	56
n	2.38	1.4	0.45	4.66	2.38

in Eq. (14) for the other material parameters, were assumed to be the same as in previous studies (Reyes et al., 2003), and are given in Table 6. The material parameters for each test were found by using the actual foam density in Eq. (14).

Fracture is modeled by eroding elements when a fracture criterion is satisfied. The criterion is based on erosion of elements when the maximum principal stress reaches a critical value:

$$\text{If } \sigma_1 \geqslant \sigma_{cr} \Rightarrow \text{erosion of element} \tag{15}$$

where σ_{cr} is the critical stress. As the tensile failure stress was approximately equal to the initial plateau stress in compression (Hanssen et al., 2002), σ_p can be used as a critical value of the principal stress. However, because of spurious noise produced by contact forces and elastic stress waves initiated when an element is eroded, the stress levels in the elements can at times be higher than the critical stress, although these should not necessarily cause fracture. To avoid premature erosion of elements, an energy-based criterion was established from Eq. (15), motivated by Cockcroft and Latham (1968), i.e.:

$$\text{If } \int_0^{\hat{\varepsilon}} H(\sigma_1 - \sigma_{cr})\sigma_1 d\hat{\varepsilon} \geqslant W \Rightarrow \text{erosion of element} \tag{16}$$

where, $H(x)$ is defined as

$$H(x) = \begin{cases} 1 & \text{if } x \geqslant 0 \\ 0 & \text{if } x < 0 \end{cases} \tag{17}$$

The critical value W used in the present study is given in Table 6. Be aware that the critical value of W may be problem dependent and it may have to be selected based on experience or validation studies using experimental data.

The material model for foam includes an option where statistical variation of foam can be chosen. The input parameters needed are C_0, C_1, and n from Eq. (14) in addition to the mean value and standard deviation of the foam density. One analysis of a foam-filled column including statistical variation of foam density was carried out. The mean density was taken as the actual density, while the standard deviation was taken as 0.0225 g/cm^3, which was used by Reyes et al. (2003).

6.2. Finite element modeling

Only half the column was modeled owing to symmetry. The extrusion was modeled with Belytschko–Tsay shell elements while the foam was modeled with standard brick elements. The load was applied at the upper end of the specimen, through a rigid body modeled with brick elements. The free length of the specimens was 199 mm, as in the experiments, and the rigid body 70 mm. All the degrees of freedom were fixed at the lower end, while the upper end was fixed to the rigid body. The model had a fine mesh; totally, 23,680 elements were used. One analysis, in which the number of elements was increased by a factor of two, was also carried out, and little effect was found on the force–displacement curve.

Table 7
Summary of results from simulations with initial imperfections

	Load angle θ [°]	Width b [mm]	Thickness h [mm]	Density ρ_f [g/cm^3]	Plateau stress σ_p [N/mm^2]	Response parameters: Peak force F_{max} [kN]	Response parameters: Mean force[a] F_{mean} [kN]	Deformation mode
S-T4-5-1.7-0	5	80	1.74	0	0	**30.45** (30.58)	**8.56** (11.67)	C
S-T4-15-1.7-0	15	80	1.74	0	0	**17.84** (17.52)	**7.35** (9.21)	C
S-T430-1.7-0	30	80	1.74	0	0	**11.40** (11.24)	**6.13** (7.95)	C
S-T4-5-1.7-1	5	80	1.74	0.123	0.52	**32.96** (31.74)	**10.95** (13.15)	C[b]
S-T4-15-1.7-1	15	80	1.74	0.118	0.46	**19.27** (18.56)	**9.16** (10.55)	C[b]
S-T430-1.7-1	30	80	1.74	0.121	0.49	**12.39** (11.42)	**7.57** (8.33)	C [b]
S-T4-5-1.7-2	5	80	1.76	0.302	4.35	**38.66** (39.51)	**21.35** (26.31)	A[**c]
S-T4-15-1.7-2	15	80	1.76	0.285	3.80	**23.26** (20.29)	**15.88** (17.0)	A[**]
S-T430-1.7-2	30	80	1.74	0.281	3.68	**14.85** (12.99)	**11.97** (11.94)	A[**]
S-T6-5-1.7-0	5	80	1.76	0	0	**55.75** (58.99)	**12.72** (16.03)	A
S-T6-15-1.7-0	15	80	1.76	0	0	**32.85** (33.12)	**10.15** (13.07)	C
S-T630-1.7-0	30	80	1.76	0	0	**20.55** (20.39)	**8.55** (11.07)	C
S-T6-5-1.7-1	5	80	1.76	0.105	0.35	**59.60** (57.4)	**13.28** (17.5)	C[c]
S-T6-15-1.7-1	15	80	1.76	0.131	0.59	**34.69** (32.63)	**11.64** (13.98)	C [b]
S-T630-1.7-1	30	80	1.76	0.12	0.49	**22.23** (20.98)	**9.46** (12.03)	C [b]
S-T6-5-1.7-2	5	80	1.77	0.301	4.30	**61.97** (66.52)	**24.46** (27.58)	A[**]
S-T6-15-1.7-2	15	80	1.77	0.311	4.67	**36.15** (36.49)	**20.05** (21.09)	A[**]
S-T630-1.7-2	30	80	1.76	0.306	4.50	**23.24** (22.32)	**15.50** (15.57)	A[**]

The values in parentheses are the corresponding values from experiments.
[a] The mean force is calculated for a displacement of 30 mm.
[b] Fracture in foam at compression side.
[c] Fracture in foam at tension side.

Guided by previous studies (Reyes et al., 2003), initial imperfections were prescribed along both the length and width of the model, to avoid too large peak forces. The initial imperfections followed the equation

$$w(x,y) = w_0 \sin\left(\frac{n\pi x}{l}\right) \sin\left(\frac{\pi y}{b-h}\right) \tag{18}$$

Here, w_0 is the amplitude, n is the number of half-sine waves along the length, b is the width and, h is the thickness of the section. Based on the studies of Reyes et al. (2002), five half-sine waves with amplitude of 0.1 mm were applied in the numerical simulations. Some analyses without initial imperfections were also carried out, mainly to examine their influence.

LS-DYNA is an explicit finite element code and the central difference method is used for the time discretization. The stability of the method depends on the time step size, and for a typical FE-mesh it can be necessary to use time steps in the order of microseconds. In order to reduce the solution time for quasi-static problems, the loading rate is often increased. To avoid introducing spurious high frequency components into the solution, the loading must be applied smoothly (Nielsen et al., 1993). Therefore, the rigid body was given a prescribed velocity field to ensure quasi-static loading. The velocity followed the function,

$$v(t) = \frac{\pi}{\pi - 2} \cdot \frac{d_{max}}{T}\left[1 - \cos\left(\frac{\pi}{2T} \cdot t\right)\right] \tag{19}$$

where d_{max} is the final displacement. T is the total duration of the loading, and was for all analyses 0.04 s. When integrated from $t = 0$ to T this expression yields d_{max} and when differentiated with respect to time, the

initial acceleration equals zero. This should ensure that the loading takes place gradually and that high frequency components in the numerical solution are avoided. Some oscillations in the load were discovered for analyses of tubes in temper T6 without initial imperfections. The analyses with initial imperfections, however, could be considered quasi-static.

6.3. Results

6.3.1. Visual observations

All the specimens collapsed globally, just as in the experiments. In the experiments, quite a number of different deformation modes were seen, but in the analyses, mainly two modes occurred. These two modes correspond to mechanism A** and C. The deformation modes of all the analyses are listed in Table 7. One can see that deformation mode A** occurs for the columns filled with the high-density foam, while the others experience mechanism C. Additionally, mechanism A was observed once, for an empty column. The three modes were actually quite similar, as they all are initiated when the compression flange buckles outward. For mechanism A, the compression flange continues to move outward, and an outward buckle is created. For mechanism C, the compression flange starts to move outwards at the same time as it moves inward just below. Then the inward deformation takes over, and an inward lobe is created. It looks as though A** simply is a variation of A, as this also is an outward buckle, but it looks a little different. When the deformation is studied more closely, it seems like the part of the flange which moves inward for mechanism C is also pushed inward for mechanism A**. However, because of the high-density foam, it cannot move inward. So only the outward lobe is created, but with a different appearance than mechanism

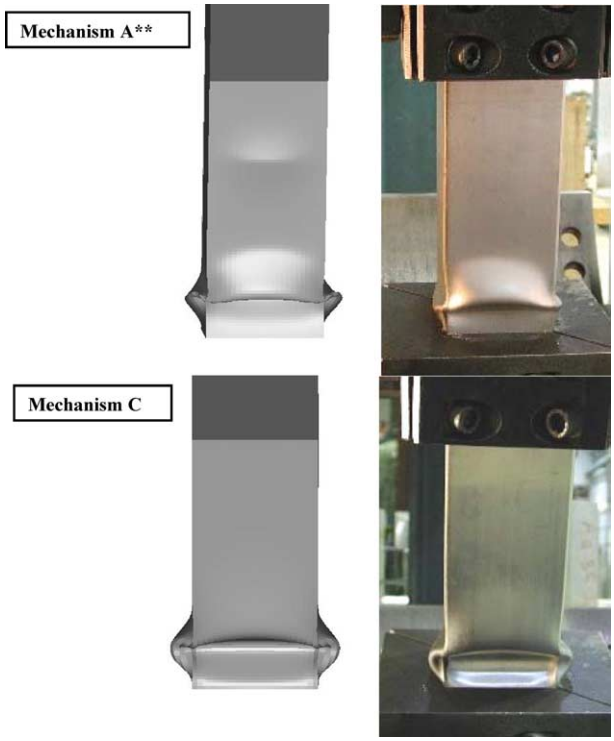

Fig. 21. Comparison of deformation modes from analyses and experiments. Pictures from experiments: S-T6-5-1.7-2-1 (A**), S-T4-15-1.7-0-3 (C).

A. Pictures from the analyses and the experiments in Fig. 21 show mechanism A** and C. As one can see, the deformation modes in the experiments and analyses are almost identical.

Fracture in the foam core occurred for many of the tubes, and this is noted in Table 7. Fig. 22 depicts how the two main deformation modes influence the extrusion and the foam core, and shows how the fracture in the foam is developed close to the clamping. The foam also fractured in the corners where the lobes in the extrusions were created in all analyses (see Fig. 23).

6.3.2. General behavior

The measured peak and mean forces from the analyses with initial imperfections are given in Table 7. The figures in parentheses are the corresponding values from the experiments. The mean loads were

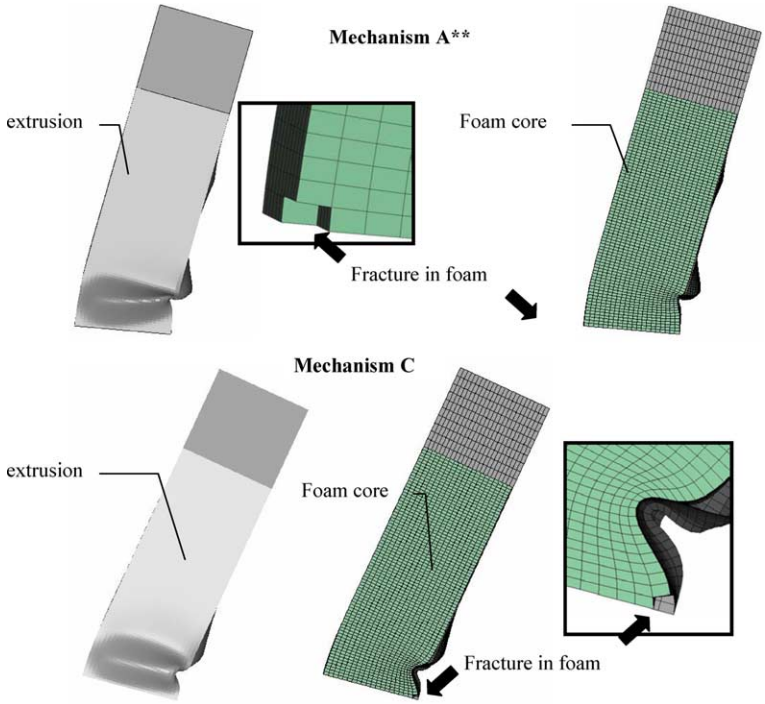

Fig. 22. Pictures from the analyses: extrusion, foam core and fracture.

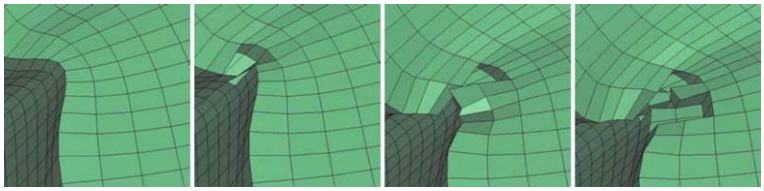

Fig. 23. The development of fracture in the foam, in the corner where the lobes in the extrusions were created.

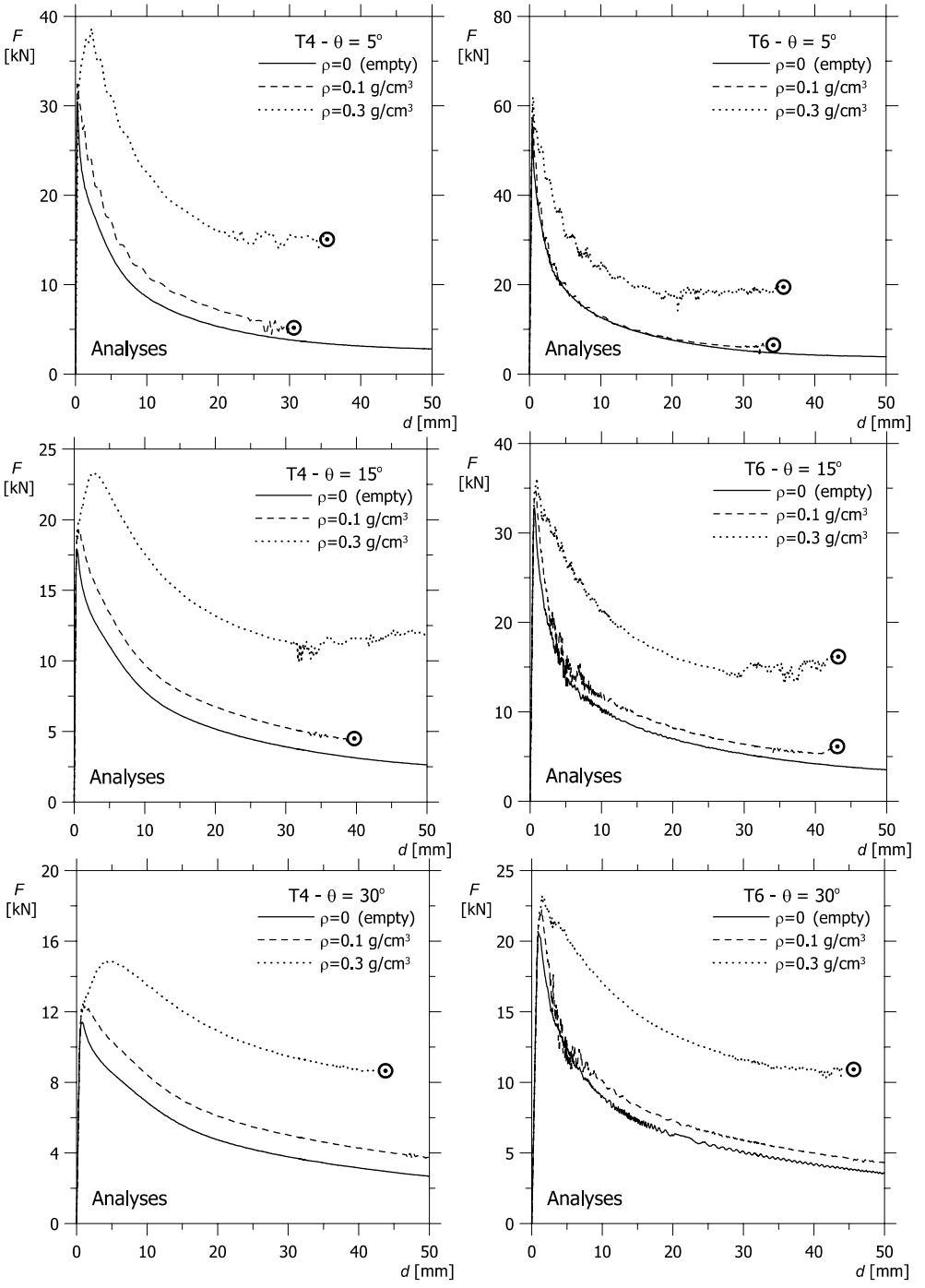

Fig. 24. Applied force vs. displacement for the numerical analyses with initial imperfections. The symbol ⊙ indicates where the analyses were stopped due to numerical problems.

calculated for a displacement of $d = 30$ mm, because most of the analyses were stopped before a deformation of 50 mm was obtained due to numerical problems related to the fracture in the foam. Fig. 24 shows typical force vs. displacement curves from the analyses. Here it is also shown when the analyses were stopped. Comparison with Fig. 12 shows that the analyses are able to predict the overall force–displacement behavior. The low-density foam has almost no influence on the force–displacement curve, while the high-density foam has a great effect. By comparing Figs. 12 and 24, it is also clear that the softening branch in the analyses is softer than for the corresponding experiments, especially for the empty columns and the tubes with a low-density foam core.

Analyses without initial imperfections were carried out in addition to the analyses with initial imperfections, and dynamics were found in the analyses of the tubes in temper T6, as in previous studies (Reyes et al., 2003). The deformation modes for the analyses with and without initial imperfections are the same. Fig. 25 shows the force–displacement curves for some typical analyses with and without initial imperfections, and as one can see, the initial imperfections do not have much influence on the force–displacement behavior. The peak loads are higher for the analyses of the tubes filled with the low-density foam without initial imperfections than in the analyses with initial imperfections. This was also the case for the empty tubes. For the tubes filled with high-density foam, there is not much difference between the analyses with and without initial imperfections.

One analysis with statistical variation of foam density and one analysis without fracture were performed to study the effect of these two features in the present problem. The force–displacement curves for the two analyses, together with the baseline analysis are shown in Fig. 25. As one can see, in this case, neither the statistical variation nor the fracture has much influence in these analyses. The standard deviation used was quite small, and the element mesh was refined, which causes the areas of different densities to be quite small. In reality, the standard deviation of the density may be larger than assumed here, and the areas with different densities may be larger. However, if this should be taken into account, further investigations of the variation of density in the foam are needed.

Correlation plots between experimental and numerical results for the peak and mean loads are given in Fig. 26. As one can see, the numerical model predicts the peak loads with good accuracy, while the mean loads are somewhat under-predicted.

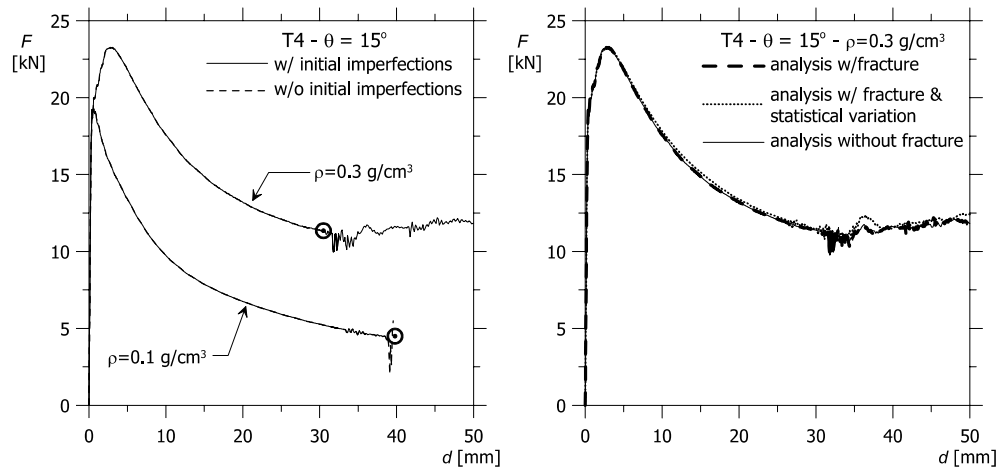

Fig. 25. Difference between analyses with and without initial imperfections, and the analyses with statistical variation and with or without fracture. The symbol ⊙ indicates where the analyses were stopped due to numerical problems.

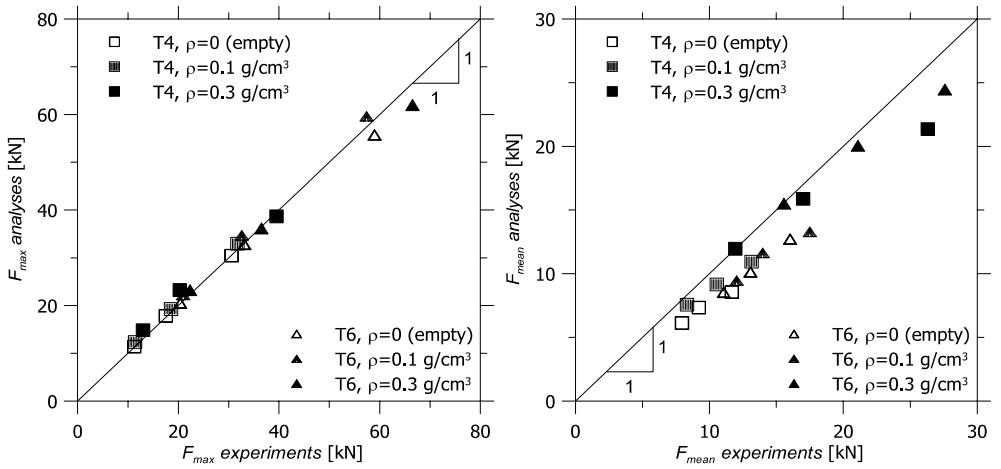

Fig. 26. Correlation between results from the experiments and numerical analyses, peak forces, and mean forces calculated at a displacement of 30 mm.

7. Concluding remarks

The crushing behavior of square aluminum tubes with aluminum foam filler subjected to oblique loading has been studied. The experiments showed that the foam filler influenced both the deformation modes and the force–displacement behavior of the columns. The lobes in the sidewalls were more localized in the foam-filled tubes than in the non-filled, and the high-density (0.3 g/cm^3) foam increased the mean loads considerably compared to the empty tubes. The low-density (0.1 g/cm^3) foam, however, had little effect on the energy absorption. The interaction curves in the present study are similar to the ones in previous studies on non-filled tubes; the failure loci shrink as the rotation progresses. However, for the columns in temper T4 with high-density foam no shrinking of the failure loci occurs.

Although the foam-filled tubes had higher energy absorption than the empty tubes, higher mean loads were also achievable by increasing the wall thickness. Four response parameters, mean force, peak force, crush force efficiency, and specific energy absorption, were examined for the foam-filled columns, and compared with results for empty columns with thicker walls. The overall trend was that the empty tubes with the same outer dimensions, but with thicker walls, gave higher values for the response parameters than the foam-filled columns with approximately the same weight. It is mentionable that the peak load, which preferably should be low, also was considerably lower for the foam-filled columns than for the empty tubes with approximately the same weight. However, when it comes to energy absorption, the empty tubes performed better than the foam-filled. The foam-filled tubes in the present study were not optimized in any respect, and in the future, it would be interesting to study whether or not an optimized foam-filled tube could perform better than an optimized non-filled column. Another way to obtain higher mass efficiency is by placing foam at the locations where the plastic hinges are expected. For a crash box that is subjected to pure axial loading as well as oblique loading, partial filling is not possible. However, if the global bending mode is foreseen, partial filling is an option that could be studied numerically.

Numerical analyses of the experiments were carried out, and the numerical model was able to predict the behavior with reasonable accuracy. The fracture and statistical variation of foam density had little influence on the results. Initial imperfections lowered the peak loads somewhat.

Acknowledgements

The authors would like to thank Hydro Automotive Structures for their generous support of the research project that forms the basis for the present work. Thanks are also given to Mr. T. Meltzer, Mr. V. Jacobsen and Mr. H. Sørlie who has provided technical assistance in the laboratory. Dr. Torodd Berstad is recognized for assistance with modeling.

References

Abramowicz, W., Jones, N., 1986. Dynamic progressive buckling of circular and square tubes. International Journal of Impact Engineering 4 (4), 243–270.

Abramowicz, W., Wierzbicki, T., 1988. Axial crushing of foam-filled columns. International Journal of Mechanical Sciences 30 (3/4), 263–271.

Ashby, M.F., Evans, A., Fleck, N.A., Gibson, L.J., Hutchinson, J.W., Wadley, H.N.G., 2000. Metal Foams: A Design Guide. Butterworth-Heineman, Woburn.

Berstad, T., Hopperstad, O.S., Langseth, M., 1994. Elasto-viscoplastic constitutive models in the explicit finite element code LS-DYNA3D. In: Second International LS-DYNA3D Conference. San Francisco.

Chen, W., 2001. Experimental and numerical study on bending collapse of aluminum foam-filled hat profiles. International Journal of Solids and Structures 38, 7919–7944.

Chen, W., Wierzbicki, T., Santosa, S., 2002. Bending collapse of thin-walled beams with ultralight filler: numerical simulation and weight optimization. Acta Mechanica 153 (3–4), 183–206.

Cockcroft, M.G., Latham, D.J., 1968. Ductility and the Workability of Metals. Journal of the Institute of Metals 96, 33–39.

Deshpande, V.S., Fleck, N.A., 2000. Isotropic models for metallic foams. Journal of the Mechanics and Physics of Solids 48, 1253–1283.

Gibson, L.J., Ashby, M.F., 1997. Cellular solids. Structure and Properties. Cambridge University Press, Cambridge.

Hallquist, J.O., 1998. Theoretical Manual. Livermore Software Technology Corporation, California.

Han, D.C., Park, S.H., 1999. Collapse behavior of square thin-walled columns subjected to oblique loads. Thin-Walled Structures 35, 167–184.

Hanssen, A.G., Langseth, M., Hopperstad, O.S., 1999. Static crushing of square aluminium extrusions with aluminium foam filler. International Journal of Mechanical Sciences 41 (8), 967–993.

Hanssen, A.G., Hopperstad, O.S., Langseth, M., 2000a. Bending of square aluminium extrusions with aluminium foam filler. Acta Mechanica 142 (1–4), 13–31.

Hanssen, A.G., Langseth, M., Hopperstad, O.S., 2000b. Static and dynamic crushing of square aluminium extrusions with aluminium foam filler. International Journal of Impact Engineering 24 (4), 347–383.

Hanssen, A.G., Langseth, M., Hopperstad, O.S., 2000c. Static and dynamic crushing of circular aluminium extrusions with aluminium foam filler. International Journal of Impact Engineering 24 (5), 475–507.

Hanssen, A.G., Langseth, M., Hopperstad, O.S., 2001. Optimum design for energy absorption of square aluminium extrusions with aluminium foam filler. International Journal of Mechanical Sciences 43 (1), 153–176.

Hanssen, A.G., Hopperstad, O.S., Langseth, M., Ilstad, H., 2002. Validation of constitutive models applicable to aluminium foams. International Journal of Mechanical Sciences 44, 359–406.

Hopperstad, O.S., Remseth, S., 1995. A return mapping algorithm for a class of cyclic plasticity models. International Journal for Numerical Methods in Engineering 38, 549–564.

Jones, N., 1989. Structural Impact. Cambridge University Press, Cambridge.

Kecman, D., 1983. Bending collapse of rectangular and square section tubes. International Journal of Mechanical Sciences 25 (9–10), 623–636.

Kim, H.-S., Wierzbicki, T., 2001. Crush behavior of thin-walled prismatic columns under combined bending and compression. Computers and Structures 79, 1417–1432.

Nielsen, K.B., Brännberg, N., Nilsson, L., 1993. Sheet metal forming simulation using explicit finite element methods. In: Structural Dynamics—EURODYN '93. Rotterdam.

Opheim, B.S., 1996. Bending of thin-walled aluminum extrusions, Doctoral Thesis. Norwegian University of Science and Technology, Trondheim.

Reid, S.R., Reddy, T.Y., Gray, M.D., 1986. Static and dynamic crushing of foam-filled sheet metal tubes. International Journal of Mechanical Sciences 28 (5), 295–322.

Reyes, A., 2003. Oblique loading of aluminum crash components, Doctoral Thesis. Norwegian University of Science and Technology, Trondheim.

Reyes, A., Langseth, M., Hopperstad, O.S., 2002. Crashworthiness of aluminum extrusions subjected to oblique loading: Experiments and numerical analyses. International Journal of Mechanical Sciences 44, 1965–1984.

Reyes, A., Langseth, M., Hopperstad, O.S., 2003. Square aluminum tubes subjected to oblique loading. International Journal of Impact Engineering 28, 1077–1106.

Reyes, A., Hopperstad, O.S., Berstad, T., Hanssen, A.G., Langseth, M., 2003. Constitutive modeling of aluminum foam including fracture and statistical variation of density. European Journal of Mechanics A/Solids 22 (6), 815–835.

Santosa, S., 1997. Crash Behavior of Box Columns Filled with Aluminum Honeycomb or Foam. Massachusetts Institute of Technology, Cambridge, MA.

Santosa, S., Wierzbicki, T., 1998. Crash behavior of box columns filled with aluminum honeycomb of foam. Computers and Structures 68, 343–367.

Santosa, S., Wierzbicki, T., 1999. Effect of an ultralight metal filler on the bending collapse of thin-walled prismatic columns. International Journal of Mechanical Sciences 41, 995–1019.

Santosa, S., Banhart, J., Wierzbicki, T., 2000. Bending Crush Resistance of Partially Foam-Filled Sections. Advanced Engineering Materials 2 (4), 223–227.

Santosa, S., Banhart, J., Wierzbicki, T., 2001. Experimental and numerical analysis of bending of foam-filled sections. Acta Mechanica 148 (1–4).

Seitzberger, M., Rammerstorfer, F.G., Degischer, H.P., Gradinger, R., 1997. Crushing of axially compressed steel tubes filled with aluminium foam. Acta Mechanica 125, 93–105.

Wierzbicki, T., Recke, L., Abramowicz, W., Gholami, T., Huang, J., 1994. Stress profiles in thin-walled prismatic columns subjected to crush loading—II. Bending. Computers and Structures 51 (6), 625–641.